Int. J. Heat Mass Transfer. Vol. 34, No. 2, pp. 389–405, 1991
Printed in Great Britain

0017–9310/91 $3.00 + 0.00

Melting of ice in a porous medium heated from below

XIAOLI ZHANG and T. HUNG NGUYEN
Department of Mechanical Engineering, Ecole Polytechnique de Montréal, Montréal, Québec, Canada H3C 3A7

and

RENÉ KAHAWITA
Department of Civil Engineering, Ecole Polytechnique de Montréal, Montréal, Québec, Canada H3C 3A7

(*Received* 18 *September* 1989 *and in final form* 28 *February* 1990)

Abstract—A numerical study is made of the melting of ice heated from below in a cavity filled with a porous medium, using the time-dependent form of the governing equations. The natural convection in the liquid phase, the conduction in the subcooled ice region, and the effect of density inversion of water are incorporated into the numerical simulation. The primary characteristics of the melting process, i.e. the onset of convection, the flow pattern in the melt, the heat transfer rate, and the interface position, are studied in terms of the Rayleigh number, the Stefan number, the aspect ratio of the cavity, and the density inversion of water. Principal findings indicate that the initial cellular pattern formed just after the onset of convection passes through several intermediate forms in its transition to a final steady state. Each change in the convection pattern is accompanied by a sudden increase in the heat transfer rate and in the displacement velocity of the solid–liquid interface. A local maximum in the heat transfer rate is exhibited shortly after the establishment of the new convection pattern.

INTRODUCTION

HEAT TRANSFER with a solid–liquid phase change is of current interest in both fundamental and applied research. Some naturally occurring examples are in the freezing and subsequent breakup of ice in lakes and rivers as well as in the melting of the upper permafrost in the Arctic due to a buried pipeline. To this may be added several other problems relevant to the areas of soil and groundwater physics. Numerous technical applications, for example, in thermal energy storage, the design of buried heat exchangers for heat pump applications, and in the food processing industry also exist. The simplest physical description of the phenomenon is of an initially solid mass that, under the influence of external heat sources, undergoes a phase change and forms a layer of liquid melt that coexists with the remaining solid phase. Subsequent evolution of the two phases will essentially depend on the behaviour of the net heat transfer to the system.

In early work, convection in the melt was neglected, and some analytical solutions were obtained such as the classic Stefan solution. However, it has been found that the conduction in the liquid is the dominant mode of heat transfer only in the early stages of melting. Subsequently, the liquid motion keeps increasing in strength, and can significantly influence the heat transfer and the position of the interface [1, 2]. The presence of the convective activity complicates analytical studies due to the fact that the interface movement is an unknown transient factor. Most of the available literature concentrates mainly on cylinders and cavities with side heating [3–12]. Recent literature reviews may be found in the articles of Viskanta [13, 14].

In this paper, a study has been made of the melting of ice heated from below in a cavity filled with a porous medium, a subject which has received relatively little attention. It is well known that convection sets in only when the effective Rayleigh number exceeds some critical value, and is generally of cellular form. As the melting proceeds, the flow pattern may persist for a period of time but the cells tend to become narrower and narrower and approach a 'transition' point, where regular cells break down, become irregular, and are finally transformed into some new regular flow pattern. The convection form, heat transfer rate and the movement of the ice–water interface during the transient phase are of primary interest. In this study, the natural convection incorporating the density inversion of water as well as the conduction in the ice region have been considered. Non-orthogonal coordinate transformations have been employed to map the two irregular time-dependent domains into rectangular regions while a finite difference method has been used to obtain the numerical results.

GOVERNING EQUATIONS

The physical system considered here is the melting of ice in a rectangular cavity containing a porous

NOMENCLATURE

a	wave number
C_p	heat capacity
g	gravitational acceleration
g_{ij}	covariant metric tensor
g^{ij}	contravariant metric tensor
Δh_f	latent heat of fusion
H	height of the cavity
J	Jacobi determinant of the coordinate transformation
k	conductivity
K	permeability
L	length of the cavity
Nu^b	average Nusselt number at the bottom surface
Nu^u	average Nusselt number at the upper surface
q	constant in the water density expression, 1.894816
R	diffusivity ratio, α^s/α^l
Ra	Rayleigh number, $\lambda g(\Delta T^l)^q KH/\nu\alpha^l$
Ra^s	Rayleigh number based on the potentially unstable layer thickness, $Ra\, S(1-\beta)^{1+q}$
S	dimensionless interface position, S^*/H
Ste^l	Stefan number of the liquid phase, $C_p^l\Delta T^l/\phi\Delta h_f$
Ste^s	Stefan number of the solid phase, $C_p^l\Delta T^s/\phi\Delta h_f(k^s/k^l)$
t	dimensionless time, $t^*/\alpha^l H^2$
T^l	dimensionless temperature in the water layer, $(T^{l*}-T_f)/\Delta T^l$
T^s	dimensionless temperature in the ice layer, $(T_f-T^{s*})/\Delta T^s$
T_b	temperature at the bottom surface
T_f	fusion temperature
T_m	maximum density temperature, 4.029325°C
T_u	temperature at the upper surface
ΔT^l	temperature difference across the melt layer, T_b-T_f
ΔT^s	temperature difference across the ice layer, T_f-T_u
u^i	contravariant velocity component
x^1, x^2	dimensionless Cartesian coordinates, $x^{1*}/H, x^{2*}/H$
XL	aspect ratio, L/H.

Greek symbols

α	diffusivity
β	$(T_m-T_f)/(T_b-T_f)$
η^1, η^2	transformed coordinates in the ice region
λ	constant in the water density expression, $9.297173\times10^{-6}\,°C^{-q}$
ν	kinematic viscosity
ξ^1, ξ^2	transformed coordinates in the water region
ρ	density
ρ_m	maximum density, 999.972 kg m^{-3}
τ	dimensionless time, t
ϕ	porosity
Φ	either T, S or φ
φ	dimensionless stream function, φ^*/α^l.

Superscripts

l	quantity in the water region
s	quantity in the ice region
*	dimensional variables.

Subscripts

c	critical value at the onset of convection
m	maximum density point.

medium. The vertical walls are insulated, the upper and lower surfaces are kept at constant temperatures T_u and T_f respectively at times less than zero. As $t \geqslant 0$, their temperatures are changed to T_u and T_b, with T_u and T_b respectively smaller and larger than the fusion temperature T_f.

As melting proceeds, a moving interface denoted here by $S(x^1, t)$ is formed. Due to the existence of this moving interface, the solid and liquid domains are irregular and time dependent. To avoid this difficulty, a curvilinear system of coordinates is used to transform the physical domain into a rectangular region for the computations. The transformations

$$x^1 = \xi^1, \quad x^2 = S\xi^2, \quad t = \tau \tag{1}$$

and

$$x^1 = \eta^1, \quad x^2 = (1-S)\eta^2 + S, \quad t = \tau \tag{2}$$

transform the two irregular regions into two rectangles

$$0 \leqslant \xi^1 \leqslant 1, \quad 0 \leqslant \xi^2 \leqslant 1 \tag{3}$$

and

$$0 \leqslant \eta^1 \leqslant 1, \quad 0 \leqslant \eta^2 \leqslant 1 \tag{4}$$

respectively. Using the two-dimensional Darcy–Boussinesq approximation, neglecting the volume change during the phase change process, and using a stream function formulation, the dimensionless momentum, energy and interface energy balance equations may be written in the curvilinear coordinate system as follows.

In the water region

$$\frac{\partial}{\partial\tau}(JT^l) + \frac{\partial}{\partial\xi^i}\left[G^{ij}\left(\hat{u}_j T^l - \frac{\partial T^l}{\partial\xi^j}\right)\right] = 0 \tag{5}$$

$$\frac{\partial}{\partial \xi^i}\left(G^{ij}\frac{\partial \varphi}{\partial \xi^j}\right)+Ra\frac{\partial}{\partial \xi^i}(J\xi^i_{x^1}|T^1-\beta|^q)=0 \quad (6)$$

where

$$J=\frac{\partial(x^1,x^2)}{\partial(\xi^1,\xi^2)}$$

$$G^{ij}=Jg^{ij}$$

$$g^{ij}=\frac{1}{J}g_{ij}(-1)^{i+j}$$

$$g_{ij}=\frac{\partial x^k}{\partial \xi^i}\frac{\partial x^k}{\partial \xi^j}$$

$$\hat{u}_j=u^k g_{kj}+g_{jk}\xi^k_t$$

$$u^1=\varphi_{\xi^2}\frac{1}{J}$$

$$u^2=-\varphi_{\xi^1}\frac{1}{J}. \quad (7)$$

The equation governing the heat conduction in the ice region takes the same form as the equations above except that T^1 is replaced by T^s, ξ by η, $\hat{u}_j$ by $g_{jk}\eta^k_t$ and the coordinate parameters are evaluated using the transform relations.

A consideration of the energy balance at the interface provides the following equation:

$$\frac{\partial S}{\partial \tau}=-Ste^l\frac{(x^1_{\xi^1})^2+(x^2_{\xi^1})^2}{x^1_{\xi^1}J^l}\frac{\partial T^l}{\partial \xi^2}\bigg|_{\xi^2=1}+Ste^s\frac{(x^1_{\eta^1})^2+(x^2_{\eta^1})^2}{x^1_{\eta^1}J^s}\frac{\partial T^s}{\partial \eta^2}\bigg|_{\eta^2=0}. \quad (8)$$

The non-linear variation of density in the water layer is given by [15]

$$\rho=\rho_m[1-\lambda|T-T_m|^q]. \quad (9)$$

The boundary conditions for the dimensionless stream function φ and dimensionless temperatures T^l and T^s are

$$T^l=1,\varphi=0, \quad \text{at} \quad \xi^2=0$$

$$T^l=\varphi=0, \quad \text{at} \quad \xi^2=1$$

$$T^l_{\xi^1}=\varphi=0, \quad \text{at} \quad \xi^1=0,1 \quad (10)$$

and

$$T^s=0, \quad \text{at} \quad \eta^2=0$$

$$T^s=-1, \quad \text{at} \quad \eta^2=1$$

$$T^s_{\eta^1}=0, \quad \text{at} \quad \eta^1=0,1. \quad (11)$$

Other parameters are defined in the Nomenclature. For a fixed choice of fluid properties, the parameters β and Ste^l are interrelated. In fact, they both remain functions of the temperature at the lower surface T_b. The parameter β, although expressed as the ratio of two temperature differences, is in fact the thickness of the upper stable layer divided by the total thickness of the melt, this being the consequence of the linear conduction profile established prior to the onset of convection. Thus a value of $\beta=0.5$ will fix the value of Ste^l at 0.1674 and implies that the thickness of the upper stable layer occupies 50% of the melt region. Ste^s represents the influence of the steadily maintained temperature at the upper surface. For example, an imposed temperature of $-4°C$ at the upper surface will give a $Ste^s=0.3068$ while a temperature of $-8°C$ will yield a value twice as large or $Ste^s=0.6136$. The definition of the Rayleigh number Ra is based on the height of the cavity and the temperature difference across the melt. A modified Rayleigh number Ra^s based on the thickness of the lower unstable layer and the temperature difference T_b-T_m across it will be defined and used later.

It should be noted that this study is based on the Darcy model where the geometric structure of the porous matrix is globally represented by the permeability K (the effect of which is incorporated into the Rayleigh number Ra). During the melting process, the porosity ϕ of the medium also influences the progression of the solid–liquid interface, as described by the energy balance, equation (8), where the Stefan number is defined as the ratio between the sensible heat and the effective latent heat of fusion ($St=C_p\Delta T/\phi\Delta h_f$). Changing the geometric matrix of the porous structure thus amounts to changing Ra or St.

For definiteness, the present study considers the phase change process of a specific fluid (water) in a given porous medium. Attention is then focused on the evolution of the various governing parameters as the temperatures of the bounding surfaces (T_u, T_b) and the dimensions of the porous layer (L, H) are changed.

SOLUTION METHOD

In order to initiate the numerical simulation, a very thin layer of melt with a constant thickness S_0 was assumed to be present. This initial condition is obtained from the Stefan solution in the melt and a linear temperature distribution in the ice region. Tests revealed that the influence of S_0 could be neglected as S_0 was sufficiently small. (Typically, $S_0=0.05$ was used in this study.)

A finite-difference method based on a control volume formulation was used to obtain the numerical solutions. The discretized equations were derived by using a power law interpolation scheme for the spatial discretization and a standard forward difference approximation for the time derivative. The use of a non-orthogonal coordinate transformation results in the appearance of cross derivative terms which were treated in a special manner to deal with instabilities [16], as described in the Appendix.

At each time step, the interface position S was determined from the energy balance at the interface. The stream function φ, temperature T^l and T^s were then simultaneously solved using an ADI technique.

The convergence criterion used was that

$$\frac{\max |\Phi_{ij}^{k+1} - \Phi_{ij}^{k}|}{\max |\Phi_{ij}^{k}|} < \varepsilon \qquad (12)$$

where Φ is either T, S or φ, superscript k is the kth iterative step and ε (10^{-4}) is the typical tolerance. The position of the interface S was then recalculated using the new values of φ and T, this procedure being repeated until converged solutions were obtained. Usually, 3–10 iterations were needed at each time step except at some critical points where the convection pattern changed rapidly and more iterations were necessary. In the present study, a 51 by 31 uniform computational grid for each domain was used with a dimensionless time step of about 10^{-2}. It was testified that the difference between the solution with larger grid number and the present solution is less than 0.5% in the scope of the present study.

The incorporation of the conductive heat transfer in the ice region results in a final steady state solution being attained, in contrast to the classical Stefan problem where the phase change process continues until the solid body is completely melted. The criterion whether steady solutions have been attained is that the difference between the two Nusselt numbers, defined at the top of the ice layer and at the bottom of the cavity, must be less than some predetermined tolerance, typically 1%. However, as will be discussed later, this criterion should be applied with care.

RESULTS AND DISCUSSION

It has been observed experimentally [2] and predicted analytically [17] that the melt remains motionless at the early stage of melting until an effective Rayleigh number exceeds some critical value. The initial appearance of convective activity has been generally observed to be of cellular form. The primary characteristics of this problem are the onset of convection, the convective pattern in the melt, the position of the interface and the heat transfer rates at the upper and lower boundaries. This study therefore concentrates on these phenomena. The influence of the Rayleigh number Ra, the temperature ratio β, the Stefan number of the liquid phase Ste^{l} (which is dependent on the temperature of the lower boundary T_b), the Stefan number Ste^{s} (dependent on the upper boundary temperature T_u) and the geometry ratio XL on the system will be discussed and illustrated. In the following, it is implied that when the influence of a parameter is being examined, the other parameters are supposed constant.

The numerical experiments performed within the scope of this study are summarized in Table 1.

Onset of convection

The primary parameter influencing the natural convection in a fluid layer heated from below is the Rayleigh number which is usually based on the thickness and the temperature difference across the potentially unstable layer. Ra^{s} is such a parameter in this study, while the symbol Ra has been reserved (as mentioned earlier) to denote the Rayleigh number based on the total thickness of the porous layer.

Table 1. Definition of investigated problems

Experiment	β	Ste^{l}	Ste^{s}	XL	Ra
1	0.2	0.4184	0.306825	1	478
2	0.2	0.4184	0.306825	1	300
3	0.2	0.4184	0.306825	1	200
4	0.2	0.4184	0.306825	1	120
5	0.2	0.4184	0.61370	1	478
6	0.4	0.2092	0.306825	1	478
7	0.5	0.1674	0.306825	1	900
8	0.5	0.1674	0.306825	1	700
9	0.5	0.1674	0.306825	1.1	700
10	0.5	0.1674	0.306825	0.8	700
11	0.5	0.1674	0.306825	1	478

Table 2 summarizes, for each experiment, the critical values of the relevant parameters at the onset of convection.

It is instructive to compare the results tabulated in Table 2 for experiments 1–4. Referring to Table 1, the overall Rayleigh number Ra for this series of experiments were respectively 478, 300, 200, and 120 with a constant value for β of 0.2. As expected, increasing the Rayleigh number results in convection being initiated at an earlier time (lower t_c) with a thinner (dimensionless) melt layer (S_c) at the critical point.

It must be noted however, that in this discussion an increase in the Rayleigh number (due to the manner in which it is defined) implies a larger cavity size, other parameters remaining fixed. A simple calculation indicates that the actual dimensional critical thickness of the melt layer *does* increase with increasing Rayleigh number, the rate of increase being marked at the lower Rayleigh numbers and tapering off at the higher Ra. One would expect therefore, that at very high Rayleigh numbers, the thickness of the melt at the onset of

Table 2. Critical values at the onset of convection

Experiment	S_c	t_c	Ra_c^s	Cell number	a
1	0.2000	0.0628	50.10	6	0.8334
2	0.3000	0.1563	47.17	4	0.8333
3	0.4426	0.4188	46.40	2	1.1297
4	0.5648	2.8000	35.56	2	0.8853
5	0.1930	0.0700	48.36	6	0.8635
6	0.3659	0.7500	39.84	4	0.6832
7	0.3127	0.7800	42.32	6	0.5330
8	0.3502	2.1250	32.96	4	0.7139
9	0.3486	1.8125	32.81	4	0.7172
10	0.3534	2.8125	33.26	4	0.7074
11		+inf		0	

convection, would be virtually independent of the Rayleigh number. This same behaviour is exhibited in the series of experiments 7, 8 and 11 which have a β value of 0.5. (Note that in experiment 11, the combination of β and Ra was such that only the pure conduction mode was realised.) It is also reasonable to speculate that, as the cavity size increases, the influence of the side walls on the critical point is being reduced due to their physical distance from the bulk of the fluid.

If now, the critical Rayleigh number Ra_c^s is computed for the unstable portion of the melt, it appears that this value increases as Ra is increased. This interesting behaviour is probably due to the fact that keeping β, Ste^l and Ste^s fixed while increasing Ra amounts to increasing the height H of the cavity as mentioned earlier. Consequently, the loss through the ice layer would be impeded with a resultant increase in the melting rate. Any small disturbance (although supposedly initially amplified exponentially according to linear stability theory) would take a finite time to manifest itself as an observable phenomenon during which time the interface has continued to move due to melting. The critical Rayleigh number Ra_c^s would thus appear to have increased due to this transient effect.

We now direct our attention to the influence of β on the onset of convection. To this end, it is useful to examine the results of experiments 1, 6 and 11 tabulated in Table 2, which have β values of 0.2, 0.4 and 0.5, respectively. These results indicate that as β increases, t_c and S_c also increase, all other quantities being constant. (It should be noted here that changing β while keeping other parameters fixed corresponds to changing both T_b and H). For $\beta = 0.5$, convection is absent so that the final steady state is in the pure conduction regime. The bottom temperature is then 8°C with an overall Rayleigh number of 478 and an effective Rayleigh number Ra^s for the unstable layer of 22.8. This value is not sufficiently large to initiate convection and therefore the only mode of heat transfer is conduction. Experiments 1 and 6 although performed at the same overall Rayleigh number Ra have descending values of the critical effective Rayleigh number Ra_c^s based on the unstable layer. The upper stable layer or 'inversion' has a 'softening' effect compared to the 'rigid' upper boundary condition as demonstrated by Oguro and Kondo [18] on the basis of a linear stability analysis.

The results of experiments 1 and 5 indicate that a higher Ste^s (lower T_u) reduces the melting rate as well as the value of the effective critical Rayleigh number Ra_c^s. Comparing the two values of S_c, it appears that the influence of Ste^s on the onset of convection is not very strong. One explanation may be the fact that in these experiments the melt is relatively very thin compared to the ice region. It may be expected that the influence of the parameter Ste^s on the onset of convection would be more pronounced for the cases where convection sets in with a larger value of S_c.

The influence of the lateral boundary on the onset of convection may be seen in the results of experiments 8, 9 and 10 where $XL = 1$, 1.1 and 0.8, respectively. From these results shown in Table 2, and Figs. 6–8, it appears that convection is developing into a symmetric, nearly square form, but narrower cells arise at higher critical effective Rayleigh number, in agreement with the fact that the lateral boundary has a stabilizing effect, as mentioned by Beck [19].

In obtaining the results presented here, it was verified that any small disturbance imposed on the system would be attenuated and die away without the inception of convection, provided that the effective Rayleigh number was subcritical. However, if the initial thickness of the melt S_0 was not small enough, convection would be initiated with a cell pattern that was strictly dependent on the form of the initial disturbance.

Convection form

The streamlines and isotherms from some of the numerical experiments are illustrated in Figs. 1–8. It can be seen that in some of them, the same cell or wave number is preserved from the inception of convection to the final steady state, while in other cases, evolution of wave number with time is evident. For convenience, this effect will be referred to as 'convection form transition'.

The time evolution of the streamlines and isotherms for experiments 1, 2 and 3, where $Ra = 478$, 300 and 200, respectively, are presented in Figs. 1–3 which indicate the influence of Ra on the convection form. For $Ra = 478$ (Fig. 1), convection is initiated with six cells, the cells becoming narrower as the melting proceeds. Subsequently, some of them shrink while others grow. Finally, the six cells break down into an irregular pattern of four cells which, however, do not persist for very long but are quickly bypassed to arrive at a two-cell configuration. The two-cell form then persists for the rest of the melting process with a steady state being attained at $S = 0.8907$. For $Ra = 300$ (Fig. 2), convection is initiated with a pattern of four cells which persist for a long time and appear to approach a sort of 'quasi' steady state. However, convection form transition occurs albeit slowly with a slight freezing in the areas of descending water flow during which a two-cell pattern gradually replaces the four-cell form. The two-cell form remains for the rest of the melting process with a steady state being obtained with $S = 0.8739$. Finally, at the lowest Rayleigh number $Ra = 200$ (Fig. 3), convection is initiated with two cells, and there is no convection form transition during the whole melting process, its steady state being approached with $S = 0.8284$.

In Fig. 5, where $\beta = 0.4$, a four-cell form was initiated and persisted for a long time in a quasi-steady state, subsequently followed by the same freezing phenomenon in areas of descending liquid. A two-cell convection form was finally established. Comparison with Fig. 1 indicates that a higher β slows down the

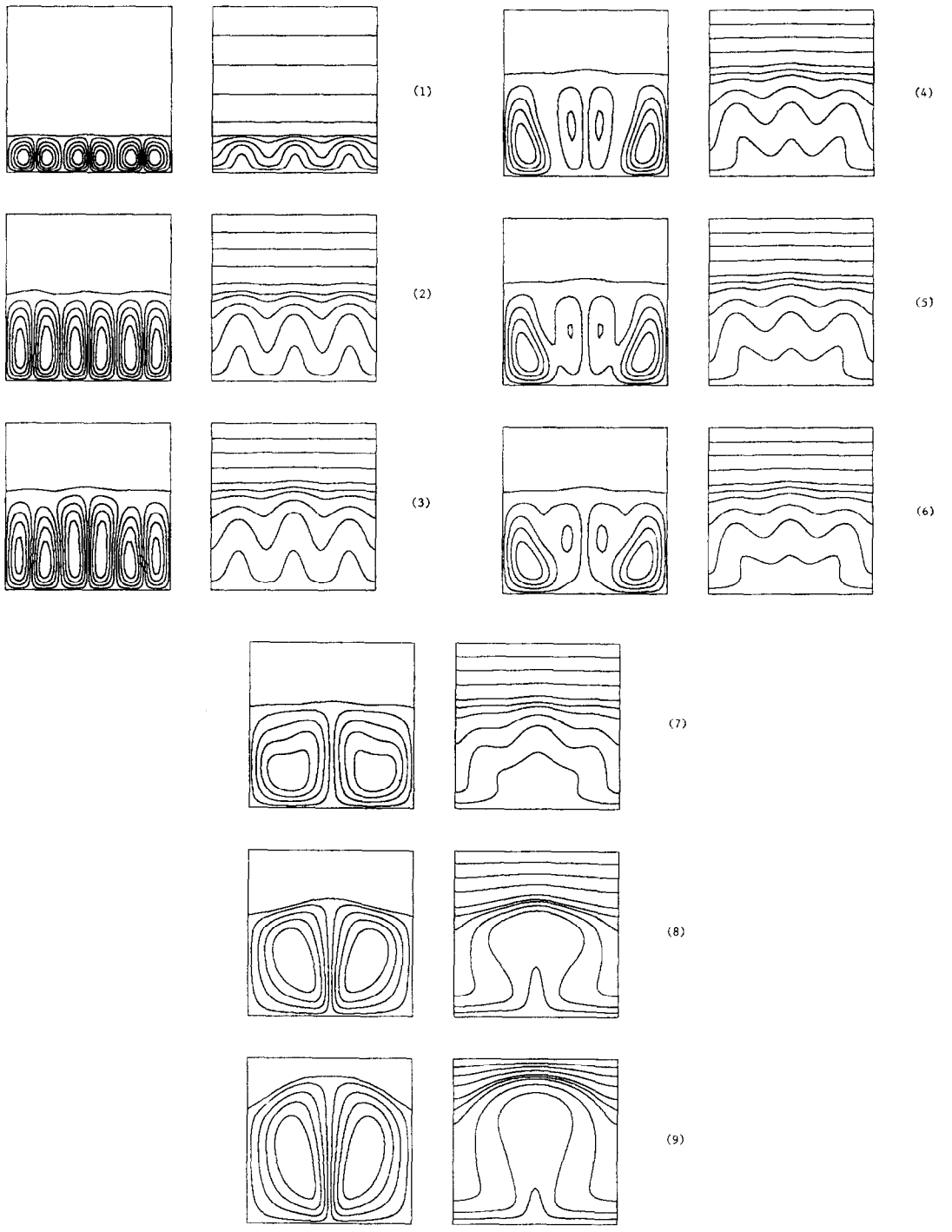

FIG. 1. Time evolution of streamlines and isotherms of Exp. 1 for $t =$ (1) 0.0772; (2) 0.2647; (3) 0.3647; (4) 0.4047; (5) 0.4077; (6) 0.4107; (7) 0.4157; (8) 0.4357; (9) 0.6357.

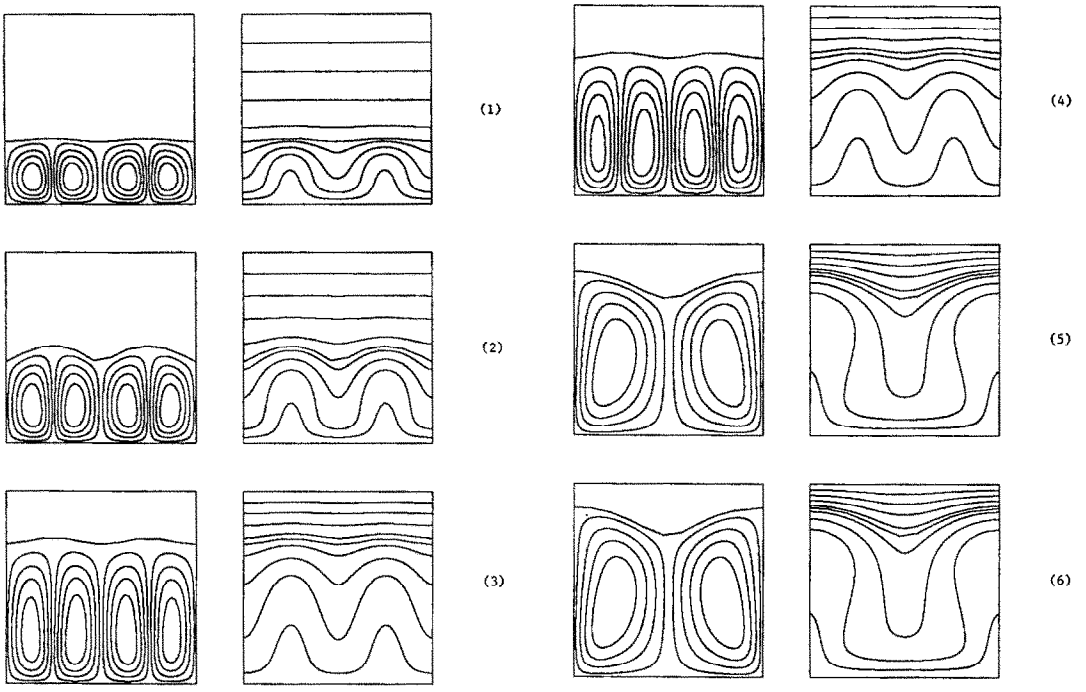

FIG. 2. Time evolution of streamlines and isotherms of Exp. 2 for t = (1) 0.2000; (2) 0.3000; (3) 1.6675; (4) 2.0675; (5) 2.7725; (6) 3.9725.

melting rate and retards the convection transition effect. Another interesting feature which may be noted in these two figures is that the convection penetrates into the upper statically stable water layer even at inception, when the thickness of the static stable layer is 1/5 and 2/5 of the total melt thickness in Figs. 1 and 5, respectively.

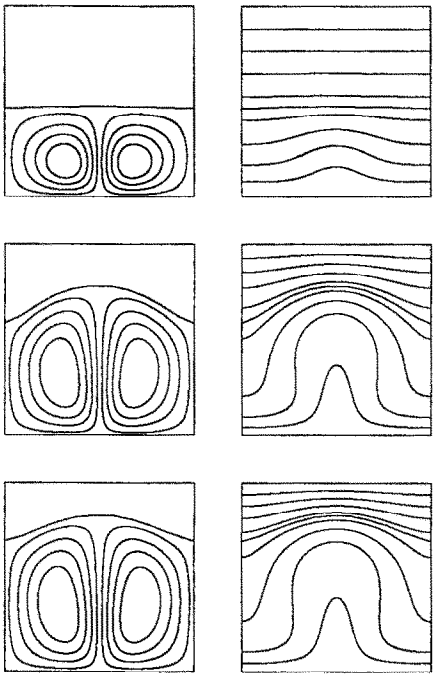

FIG. 3. Time evolution of streamlines and isotherms of Exp. 3 for t = (1) 0.5000; (2) 0.9000; (3) 1.500.

The influence of Ste^s on the cell pattern can be seen in Figs. 1 and 4. Figure 4 presents the convective history of experiment 5 in which all relevant parameters are the same as in experiment 1 except for Ste^s. The two convection forms are very similar, the only difference being a slight time lag at the early stage of convection. At this time, the melt is much thinner than the ice region so that the influence of the upper temperature on the water region would be small. The convection patterns evolve in different ways as further melting proceeds with a demonstrated dependence on the Ste^s parameter. For $Ste^s = 0.3068$, the convection form transition occurs earlier, quickly passing through an irregular four-cell pattern and terminating with a two-cell pattern. For $Ste^s = 0.61036$, the initial form persists during a long quasi-steady period. The convection form transition happens much later with the attendant refreezing phenomenon mentioned earlier. The six-cell form is transformed into a four-cell pattern and no further transition is observed afterwards. Clearly, the Ste^s parameter has an increasing effect on the convection pattern as further melting develops.

It is reasonable to expect that more than one convection form transition may exist if the convective activity in the water layer was enhanced, for example, by increasing Ra, or decreasing β or Ste^s, which would result in more convection cells being initiated at the onset with smaller values for S_c.

The cause and the 'preferred' wave number of the

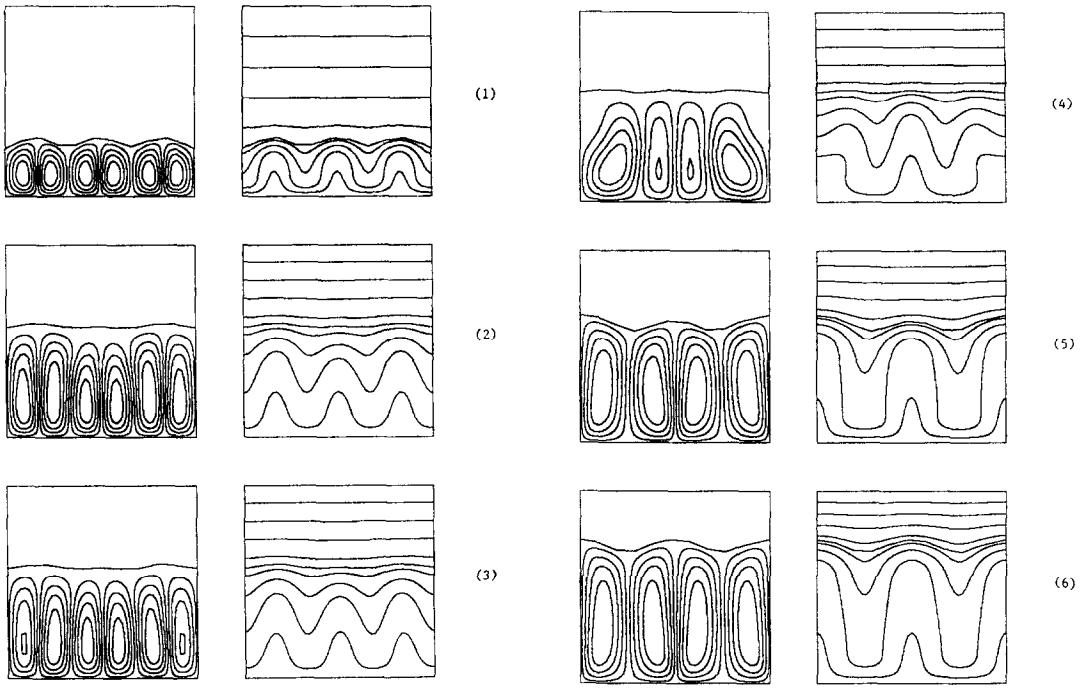

FIG. 4. Time evolution of streamlines and isotherms of Exp. 5 for t = (1) 0.1284; (2) 0.8399; (3) 0.8599; (4) 0.8999; (5) 0.9499; (6) 1.3499.

new convection pattern after the convection form transition, are interesting questions. It was predicted by Clever and Busse [20], and also by Strauss [21] that a secondary stability problem exists after the onset of convection in the Bénard problem. They pointed out that the two-dimensional convection solutions are unstable when the (Ra^s, a) point lies outside their stability envelope. The convection form transition observed in this study may be the result of unstable convection forms being encountered during the melting process. As the fluid layer becomes thicker, the convection cells become narrower so that at some point it is possible that a certain unstable bandwidth which is very sensitive to this convection form, is encountered. It was verified that the point (Ra^s, a) where convection form transition began to appear was out of Strauss's stability balloon.

As mentioned earlier, the initial convection form appeared to be strictly dependent on the initial melt thickness S_0 and the initial disturbance if S_0 is not very small. In order to verify if the final steady solutions were still dependent on these initial conditions, some further tests were performed for experiment 8. One such test was to start the simulation with an initial melt of $S_0 = 0.35$ and a disturbance which could initiate a three-cell convection pattern. It was observed that convection was initiated with a three-cell pattern which was later replaced by a two-cell form and the steady solution was obtained as before. Another test was the simulation of freezing from above. A thin layer of ice and pure conduction in the water layer were used as the initial conditions. A two-cell pattern was initiated, which was subsequently replaced by a four-cell pattern as the freezing continued, the steady solution obtained being identical to the previous case. Therefore, it can be concluded that the final steady solutions (the interface position, the convection form and the heat transfer rate) were independent of the initial conditions.

Heat transfer rate and interface position

The lower and upper Nusselt numbers are defined as

$$Nu^b = \frac{1}{XL}\int_0^{XL} T^l_{\xi^2}/S|_{\xi^2=0}\,\mathrm{d}\xi^1 \qquad (13)$$

and

$$Nu^u = Ste^s/Ste^l \frac{1}{XL}\int_0^{XL} T^s_{\eta^2}/(1-S)|_{\eta^2=1}\,\mathrm{d}\eta^1 \qquad (14)$$

respectively.

Figures 9–12 indicate the variation of the average interface position and Nusselt numbers vs time for several experiments. Some jumps may be observed during the melting process, the earliest one corresponding to the point of initiation of convection, while others (if they exist) to the convection form transition. These periods are accompanied by a sharp increase in both the interface movement and in the heat transfer rates. It appears that the convection form

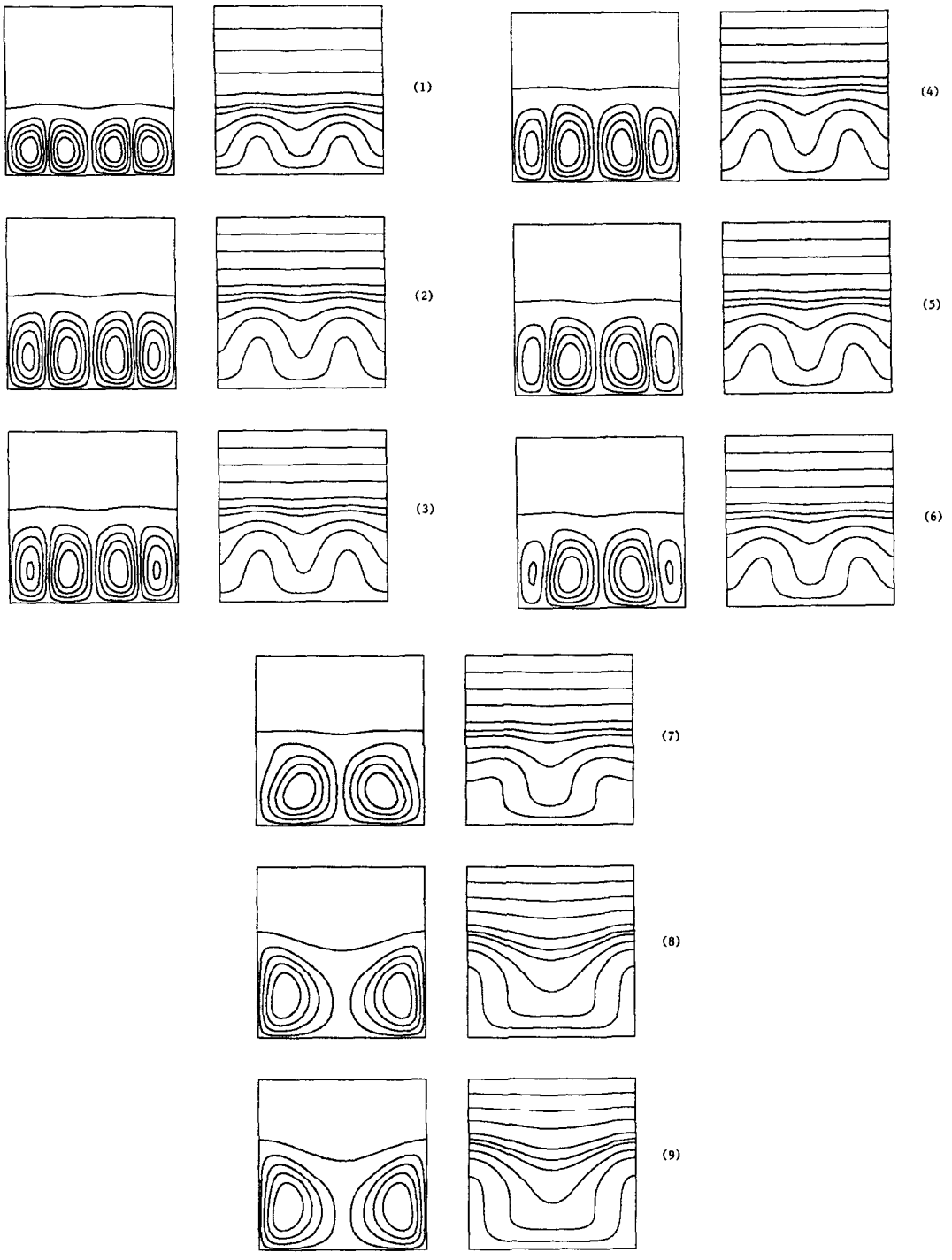

FIG. 5. Time evolution of streamlines and isotherms of Exp. 6 for t = (1) 0.9390; (2) 3.3339; (3) 3.4390; (4) 3.5390; (5) 3.6040; (6) 3.6340; (7) 3.6640; (8) 3.8640; (9) 5.3640.

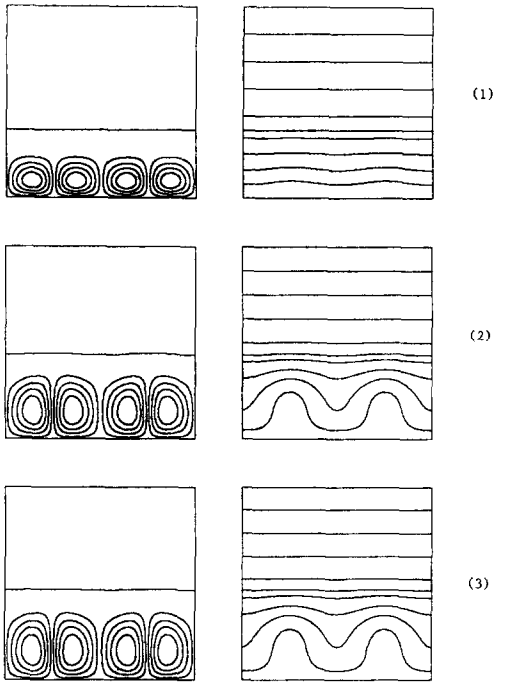

FIG. 6. Time evolution of streamlines and isotherms of Exp. 8 for t = (1) 0.1000; (2) 3.2815; (3) 5.2815.

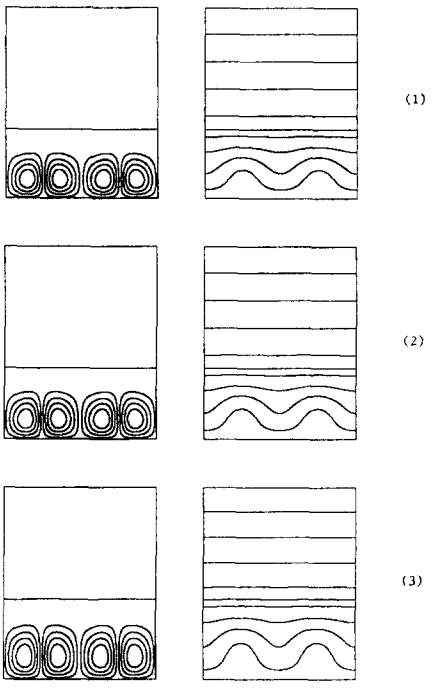

FIG. 8. Time evolution of streamlines and isotherms of Exp. 10 for t = (1) 2.9330; (2) 3.0830; (3) 4.5430.

transition to a new cell pattern occurs in order to enhance the melting process.

The influence of β, Ste^s, XL on the heat transfer rate and interface position can be seen in Figs. 10–12, respectively. Higher β, Ste^s, and lower XL have stabilizing effects, they reduce the heat transfer rates, slow down the interface movement, postpone or even eliminate the convection form transition.

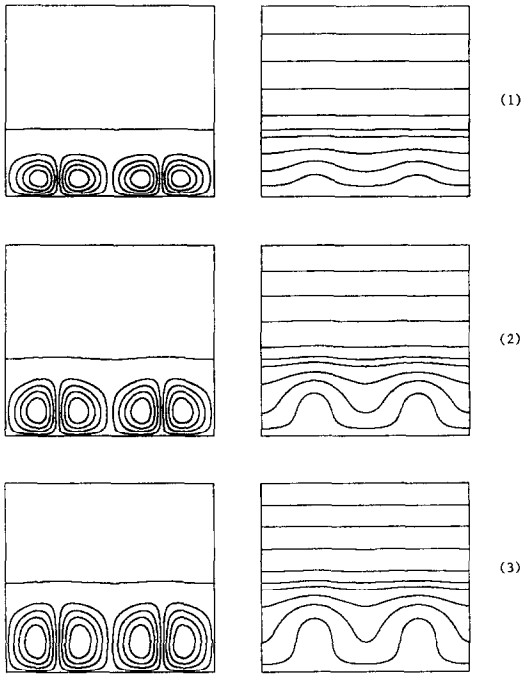

FIG. 7. Time evolution of streamlines and isotherms of Exp. 9 for t = (1) 2.5830; (2) 3.0830; (3) 5.3580.

Figures 9 and 11 indicate two types of convection form transition. One occurs at a time when the two Nusselt numbers are very different, the other one at a time long after an apparent steady state is approached. It was observed that slight refreezing in certain regions of the water layer occurs before and during a convection form transition of the second type but is absent during the evolution of the first type (Figs. 2, 4, 5, 10, especially Figs. 5 and 10).

The convergence of the two Nusselt numbers cannot therefore be used as a unique criterion to determine the approach to the final steady solution. Other aspects such as whether the cells have the same size and shape, and the position of the (Ra^s, a) point with respect to Strauss's stability envelope, have to be considered simultaneously with the convergence of the two Nusselt numbers in order to ascertain if a true steady state has been reached.

Finally, results at the steady state using only the pure conduction mode, and with convection, are presented in Table 3 to show the overall effects of convection on the interface position and the heat transfer rates.

CONCLUDING REMARKS

The melting of ice heated from below in a rectangular cavity filled with a porous medium has been investigated numerically. In the melting process, con-

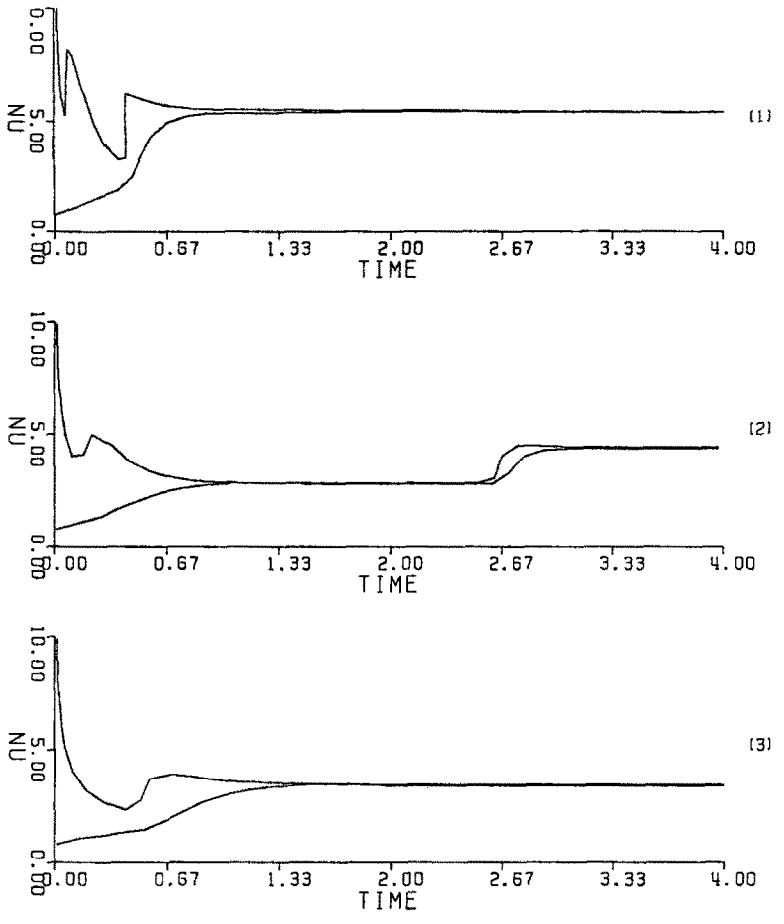

FIG. 9.1. Influence of Rayleigh number on heat transfer rate: (1) $Ra = 478$, Experiment 1; (2) $Ra = 300$, Experiment 2; (3) $Ra = 200$, Experiment 3.

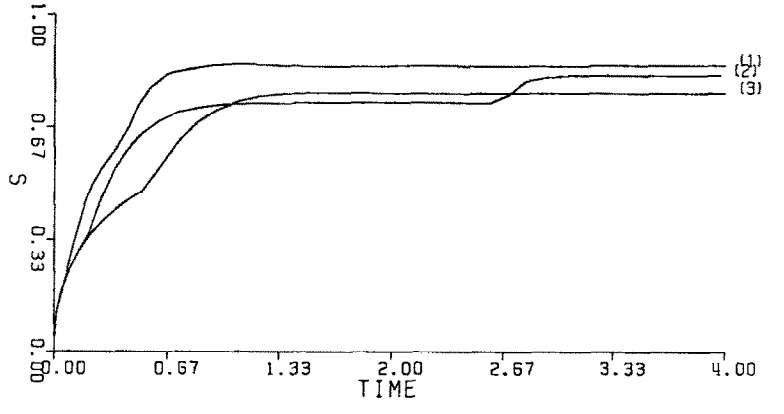

FIG. 9.2. Influence of Rayleigh number on interface position: (1) $Ra = 478$, Experiment 1; (2) $Ra = 300$, Experiment 2; (3) $Ra = 200$, Experiment 3.

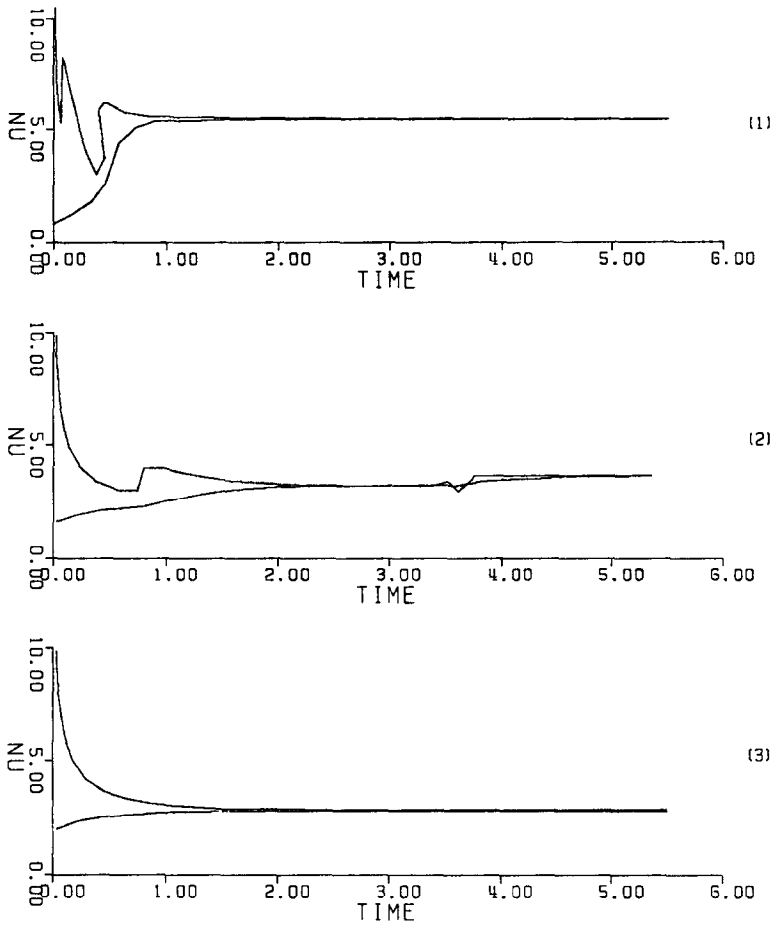

FIG. 10.1. Influence of β on heat transfer rate: (1) $\beta = 0.2$, Experiment 1; (2) $\beta = 0.4$, Experiment 6; (3) $\beta = 0.5$, Experiment 11.

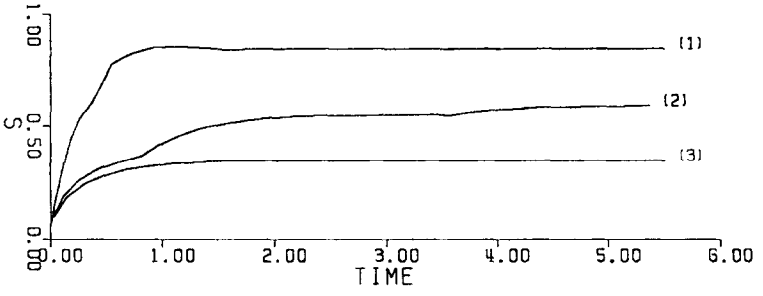

FIG. 10.2. Influence of β on interface position: (1) $\beta = 0.2$, Experiment 1; (2) $\beta = 0.4$, Experiment 6; (3) $\beta = 0.5$, Experiment 11.

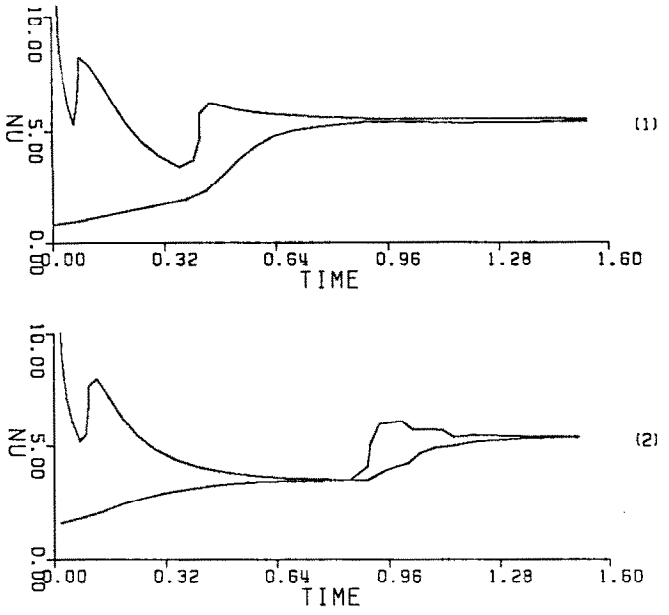

FIG. 11.1. Influence of Ste^s on heat transfer rate: (1) $Ste^s = 0.3068$; Experiment 1; (2) $Ste^s = 0.6136$, Experiment 5.

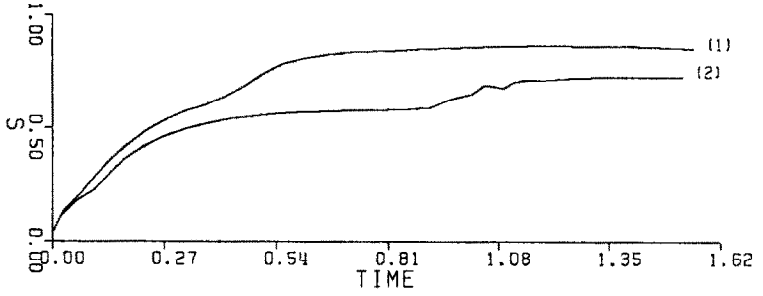

FIG. 11.2. Influence of Ste^s on interface position: (1) $Ste^s = 0.3068$; Experiment 1; (2) $Ste^s = 0.6136$, Experiment 5.

vection starts to play an important role as the melt thickness attained a certain value corresponding to the critical Rayleigh number for the onset of convection. The newly formed convection cells appear to have a nearly square form. As melting continues, these cells become more slender, and suddenly break up sequentially. The transition period (i.e. duration of the breaking process) is quite short, but is followed by a very long (i.e. quasi-steady) period. The final steady state (which in fact exists when the upper boundary is maintained at a temperature below the melting point) is sometimes difficult to attain as it can be preceded by very long quasi-steady states. This phenomenon is reflected in the evolution of the heat transfer rate. The curve of Nusselt number vs time exhibits a jump each time a convection cell disappears. It is therefore reasonable to conclude that the new convection pattern is formed to augment the heat transfer, in agreement with the principle of maximum heat transfer proposed by Malkus. This change in the convection pattern may be interpreted with reference to the stability theory of Busse. As melting continues, the convection cells become narrower and narrower until a point is reached where they become unstable with respect to a certain kind of perturbation and cannot survive. This is in fact the point at which increasing wave number crosses threshold to fall outside Busse's stability balloon. Moreover, during the transition from one flow pattern to another, the inverse phenomenon of refreezing was sometimes observed together with a decrease in the heat transfer rate.

A final remark should be made concerning the specific melting of ice. Here the melt is comprised of a

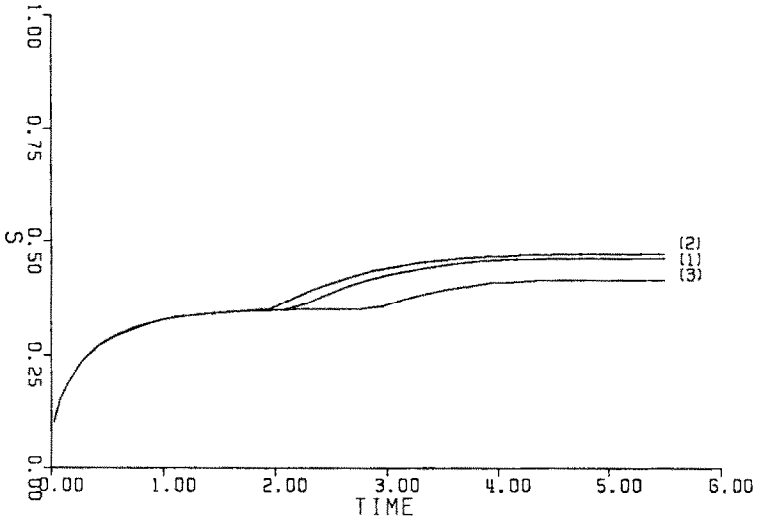

FIG. 12.1. Influence of XL on heat transfer rate: (1) $XL = 1.0$, Experiment 8; (2) $XL = 1.1$, Experiment 9; (3) $XL = 0.8$, Experiment 10.

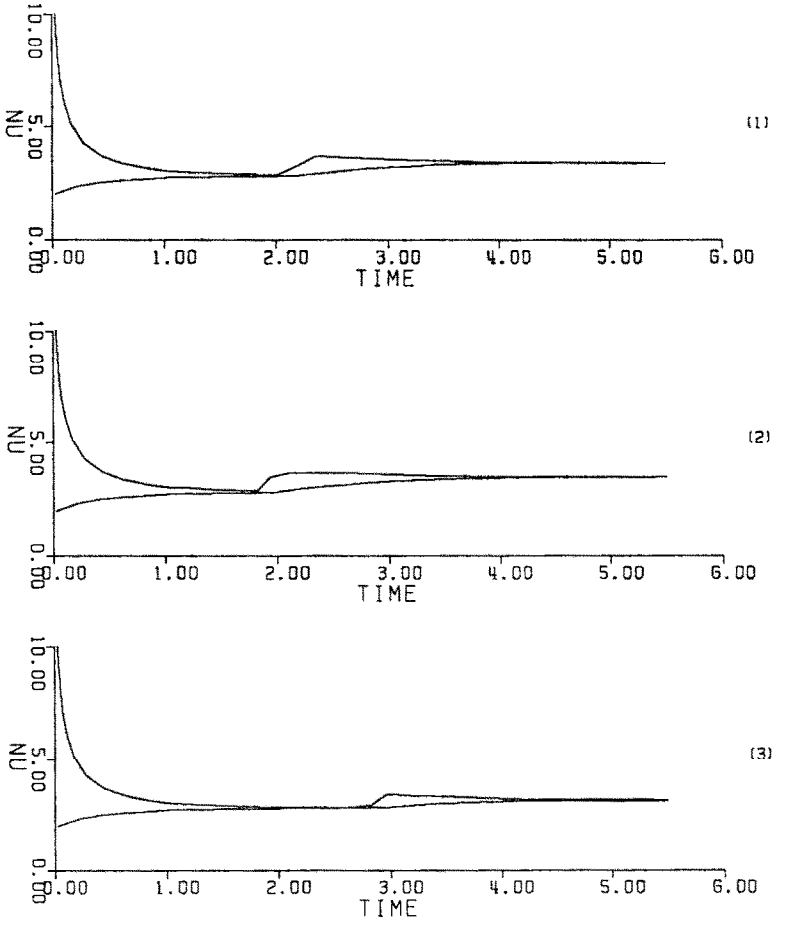

FIG. 12.2. Influence of XL on interface position: (1) $XL = 1.0$, Experiment 8; (2) $XL = 1.1$, Experiment 9; (3) $XL = 0.8$, Experiment 10.

Table 3. Steady solution results using conduction mode only and with convection

Experiment	S_{cond}	S_{conv}	Nu_{cond}	Nu_{conv}	S_{min}	S_{max}
1	0.5769	0.8449	1.7333	5.5100	0.6886	0.8907
2	0.5769	0.8184	1.7333	4.4370	0.7273	0.8739
3	0.5769	0.7673	1.7333	3.4830	0.6887	0.8284
5	0.4054	0.7220	2.4667	5.3740	0.6794	0.7465
6	0.4054	0.5897	2.4667	3.680	0.5225	0.6471
8	0.3530	0.4650	2.8329	3.4170	0.4603	0.4678
9	0.3530	0.4739	2.8329	3.486	0.4647	0.4778
10	0.3530	0.4177	2.8329	3.184	0.4164	0.4191
11	0.3530	0.3530	2.8329	2.8329	0.3530	0.3530

stable layer of cold water (below 4°C) lying between the ice surface and an unstable layer of warmer water (above 4°C). As a consequence, if the lower surface is maintained at a temperature below 4°C, no convection would occur. The presence of a stable layer adjacent to the ice surface also greatly reduces the heat transfer, and thereby the melting rate, when the heated surface is maintained at temperatures below 10°C. Furthermore, the cold stable water at the ice surface also attenuates the effect of the impinging flow rising from the unstable layer. Thus the water–ice interface, when heated from below, is less wavy than when heated from above.

Acknowledgement—This study was supported by the Natural Sciences and Engineering Research Council of Canada under grant No. OGP 0000626.

REFERENCES

1. D. V. Boger and J. W. Westwater, Effect of buoyancy on the melting and freezing process, *J. Heat Transfer* **89**, 81–89 (1967).
2. C. Gau and R. Viskanta, Effect of natural convection on solidification from above and melting from below of a pure metal, *Int. J. Heat Mass Transfer* **28**, 573–587 (1985).
3. C. Beckman and R. Viskanta, Natural convection solid/liquid phase change in porous media, *Int. J. Heat Mass Transfer* **31**, 35–46 (1988).
4. C. J. Ho and S. Chen, Numerical simulation of melting of ice around a horizontal cylinder, *Int. J. Heat Mass Transfer* **29**, 1359–1369 (1986).
5. C. J. Ho and R. Viskanta, Heat transfer during melting from an isothermal vertical wall, *J. Heat Transfer* **106**, 12–19 (1984).
6. B. W. Webb and R. Viskanta, Analysis of heat transfer during melting of a pure metal from an isothermal vertical wall, *Numer. Heat Transfer* **9**, 539–558 (1986).
7. M. Okada and R. Fukumoto, Melting around a horizontal pipe embedded in a frozen porous medium, *Trans. Japan Soc. Mech. Engrs* **48B**, 2041–2049 (1982).
8. M. Okada, Analysis of heat transfer during melting from a vertical wall, *Int. J. Heat Mass Transfer* **27**, 2057–2066 (1984).
9. M. Kazmierczak, D. Poulikakos and D. Sadowski, Melting of a vertical plate in porous medium controlled by forced convection of a dissimilar fluid, *Int. Commun. Heat Mass Transfer* **14**, 507–518 (1987).
10. M. Kazmierczak, D. Poulikakos and I. Pop, Melting from flat plate embedded in a porous medium in the presence of steady natural convection, *Numer. Heat Transfer* **10**, 571–581 (1986).
11. P. Jany and A. Bejan, The scales of melting in the presence of natural convection in a rectangular cavity filled with porous medium, *J. Heat Transfer* **110**, 526–529 (1988).
12. A. Bejan, Theory of melting with natural convection in an enclosed porous medium, *J. Heat Transfer* **111**, 407–415 (1989).
13. R. Viskanta, Phase change heat transfer. In *Solar Heat Storage: Latent Heat Materials* (Edited by G. A. Lane), Vol. 1. CRC Press, Boca Raton, Florida (1983).
14. R. Viskanta, Natural convection in melting and solidification. In *Natural Convection: Fundamentals and Applications* (Edited by S. Kakaç, W. Aung and R. Viskanta). Hemisphere, Washington, DC (1985).
15. B. Gebhart and J. Mollendorf, A new density relation for pure and saline water, *Deep-Sea Res.* **124**, 831–848 (1977).
16. X. Zhang, Wavenumber selection in penetrative convection, Ph.D. thesis, Ecole Polytechnique de l'Université de Montréal, Montréal, Québec (1989).
17. E. M. Sparrow and N. Shamsundar, Convective stability in a melting layer heated from below, *J. Heat Transfer* **98**, 88–94 (1976).
18. Y. Ogura and H. Kondo, A linear stability of convective motion in a thermally unstable layer below a stable region, *J. Met. Soc. Japan* **48**, 204–215 (1970).
19. J. E. Beck, Convection in a box of porous material saturated with fluid, *Physics Fluids* **15**(8), 1377–1383 (1972).
20. R. M. Clever and F. H. Busse, Transition to time-dependent convection, *J. Fluid Mech.* **65**(4), 625–645 (1974).
21. J. M. Strauss, Large amplitude convection in a porous media, *J. Fluid Mech.* **64**, 51–63 (1974).

APPENDIX

The use of a non-orthogonal coordinate transformation results in the appearance of cross-derivative terms which have to be treated in a special manner so as to deal with instabilities. Denoting the relevant contravariant components of the flux as

$$J^{ij}(\Phi) = G^{ij}\left(\hat{u}_j\Phi - r\frac{\partial\Phi}{\partial\xi^j}\right) \text{ (no summation here)} \qquad \text{(A1)}$$

where Φ can be either T or φ, r equals 1 as Φ represents T^1 and φ, and r equals R as Φ represents T^*. The diffusion–convection equation may then be written as

$$\frac{\partial}{\partial t}(J\Phi) + \frac{\partial}{\partial\xi^i}(J^{i1}(\Phi) + J^{i2}(\Phi)) = 0. \qquad \text{(A2)}$$

Integrating on the control volume as shown in Fig. A1 yields

$$\frac{J\Phi - J^0\Phi^0}{\Delta t}\Delta x\Delta y|_P + [J^{11}(\Phi)+J^{12}(\Phi)]\Delta y|_w^e + [J^{21}(\Phi)+J^{22}(\Phi)]\Delta x|_s^n = 0 \quad (A3)$$

where P represents the current point under discussion, E, W, N, S the neighbours of P to the east, west, north and south, respectively, and e, w, n, s are the mid points of the control volume interface.

The values of J^{ii} are approximated using the power law scheme. For example, the value of the non-cross term J^{11} at point e is approximated using the power law scheme directly as

$$J^{11}(\Phi)|_e = G^{11}[(\hat{u}_1 + b_1)\Phi_P - b_1\Phi_E]|_e \quad (A4)$$

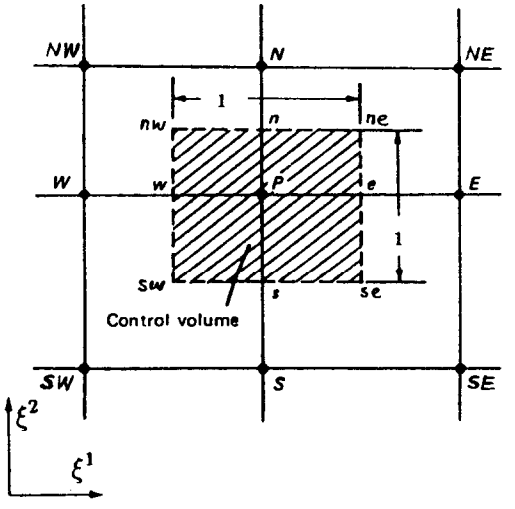

FIG. A1. Sketch of control volume.

where

$$b_1 = \max\{0, -\hat{u}_1\} + \max\left\{0, \left(1 - 0.1\left|\frac{\hat{u}_1}{r}\right|\right)^5\right\}\Big|_e. \quad (A5)$$

Similarly, the term $J^{12}(\Phi)$ at point e may also be represented as

$$J^{12}(\Phi)|_e = G^{12}[(\hat{u}_2 + b_2)\Phi_{i+1/2,j-1/2} - b_2\Phi_{i+1/2,j+1/2}]|_e \quad (A6)$$

where

$$b_2 = \max\{0, -\hat{u}_2\} + \max\left\{0, \left(1 - 0.1\left|\frac{\hat{u}_2}{r}\right|\right)^5\right\}. \quad (A7)$$

$\Phi_{i+1/2,j-1/2}$ and $\Phi_{i+1/2,j+1/2}$ are interpolated as

$$\Phi_{i+1/2,j-1/2} = \begin{cases} \frac{1}{2}(\Phi_{i,j} + \Phi_{i+1,j-1}) & \text{if } G^{12} < 0 \\ \frac{1}{2}(\Phi_{i+1,j} + \Phi_{i,j-1}) & \text{if } G^{12} > 0 \end{cases} \quad (A8)$$

and

$$\Phi_{i+1/2,j+1/2} = \begin{cases} \frac{1}{2}(\Phi_{i,j+1} + \Phi_{i+1,j}) & \text{if } G^{12} < 0 \\ \frac{1}{2}(\Phi_{i,j} + \Phi_{i+1,j+1}) & \text{if } G^{12} > 0 \end{cases}. \quad (A9)$$

These interpolations were obtained from geometric arguments. Since

$$G^{12} = -\frac{1}{J}g_{12} = -\frac{1}{J}\mathbf{e}_1 \cdot \mathbf{e}_2 \quad (A10)$$

$G^{12} < 0$ means that the angle between the directions $\mathbf{e}_1$ and $\mathbf{e}_2$ is smaller than $\pi/2$ and therefore, the position at '$(i+1/2, j-1/2)$' is closer to the points P and $(i+1, j-1)$ than to the points S and E. The inverse conclusion may also be made for a positive value of G^{12}. One may show that, the interpolations in equations (A8) and (A9) further ensure that the coefficients of the discretized equations

$$a_p\Phi_p = \sum a_{nb}\Phi_{nb} \quad (A11)$$

usually satisfy the rules of discretization in order to avoid the instability caused by the cross terms under the non-orthogonal curvilinear coordinate.

FUSION DE LA GLACE DANS UN MILIEU POREUX CHAUFFE PAR LE BAS

Résumé—Un étude numérique est faite sur la fusion de la glace chauffée par le bas dans une cavité remplie par un milieu poreux, en considérant les équations sous la forme dépendant du temps. On introduit dans la simulation numérique la convection naturelle dans la phase liquide, la conduction dans la glace sous-refroidie et l'effet de l'inversion de densité de l'eau. Les caractéristiques principales du mécanisme de fusion, c'est-à-dire l'apparition de la convection, la configuration de l'écoulement dans le bain, les flux thermiques et la position de l'interface sont étudiées en fonction du nombre de Rayleigh, du nombre de Stefan, du rapport de forme. Les principaux résultats montrent que la configuration cellulaire initiale formée juste après l'apparition de la convection passe à travers plusieurs formes intermédiaires depuis la transition jusqu'à un état final. Chaque changement dans la configuration de convection est accompagné d'un accroissement brutal du transfert thermique et d'une vitesse de déplacement de l'interface solide–liquide. Un maximum local de la densité de flux thermique apparaît brièvement après l'établissement d'une nouvelle configuration de convection.

DAS SCHMELZEN VON EIS IN EINEM VON UNTEN BEHEIZTEN PORÖSEN MEDIUM

Zusammenfassung—Das Schmelzen von Eis in einem von unten beheizten Hohlraum, der ein poröses Medium enthält, wird unter Verwendung der zeitabhängigen Erhaltungsgleichungen numerisch untersucht. Die numerische Lösung enthält Einflüsse der natürlichen Konvektion in der flüssigen Phase, der Wärmeleitung im Gebiet unterkühlten Eises sowie den Einfluß der Dichteinversion bei Wasser. Die Haupteigenschaften des Schmelzvorgangs, nämlich das Einsetzen von Konvektion, die Strömungsform in der Schmelze, der Wärmeübergang und die Position der Schmelzfront werden in Abhängigkeit von der Rayleigh-Zahl, der Stefan-Zahl, vom Seitenverhältnis des Hohlraums sowie von der Dichteinversion des Wassers untersucht. Die wichtigsten Ergebnisse zeigen, daß die anfänglich vorhandene zellförmige Struktur unmittelbar nach Einsetzen der Konvektion sich verändert und nach einigen Zwischenstadien schließlich zu einem stationären Endzustand hin führt. Jede Änderung der Form der Konvektion ist mit einer plötzlichen Zunahme des Wärmeübergangs und der Wanderungsgeschwindigkeit der Fest-Flüssig-Phasengrenze verbunden. Kurz nach Erreichen einer neuen Konvektionsform ergibt sich ein örtliches Maximum des Wärmeübergangs.

ТАЯНИЕ ЛЬДА В НАГРЕВАЕМОЙ СНИЗУ ПОРИСТОЙ СРЕДЕ

Аннотация—С использованием нестационарных уравнений численно исследуется таяние нагреваемого снизу льда в полости, заполненной пористой средой. Численное моделирование включает естественную конвекцию в жидкой фазе, теплопроводность в недогретой области льда, а также эффект инверсии плотности-воды. Основные характеристики процесса таяния, а именно, возникновение конвекции, структура потока в расплаве, интенсивность теплопереноса и расположение межфазной границы, исследуются на основе чисел Рэлея и Стефана, а также соотношения сторон полости и инверсии плотности волы. Полученные результаты свидетельтвуют о том, что начальная структура ячеек, образованная непосредственно после возикновения конвекции, при переходе к стационарному состоянию проходит несколько промежуточных видов. Каждое изменение режима конвекции сопровождается резким увеличением интенсивности теплопереноса и скорости смещения границы раздела твердое тело–жидкость. Локальное максимальное значение интенсивности теплопереноса проявляется вскоре после установления нового режима конвекции.